Black Diamonds from Marange (Zimbabwe): A Result of Natural Irradiation and Graphite Inclusions

Karen V. Smit, Elina Myagkaya, Stephanie Persaud, and Wuyi Wang

This study investigates the color origin of 40 natural Fancy Dark brown-black round brilliant diamonds from the Marange alluvial deposits in eastern Zimbabwe. Visual observations show that the dark appearance of the Marange diamonds is due to a combination of graphite micro-inclusions (associated with methane), graphite needles, and dark brown radiation stains that occur along internal fractures. The GR1 (V^0) defect, typically formed during natural and artificial irradiation, is observed in the optical spectra of 43% of the diamonds, although its intensity is too low to significantly impact the bodycolor. Natural irradiation in these diamonds is likely related to their billion-year residence in the Umkondo conglomerate, which is known to contain radioactive minerals such as zircon. Aside from radiation staining, irradiation-damaged diamond appears non-luminescent in DiamondView images and shows a weaker, broader diamond peak (at 1332 cm^{-1}) in Raman spectroscopy. Brown coloration of the radiation stains is due to heating of the diamonds during later regional metamorphism, which also facilitated the formation of the H3 (NVN^0) and NiN complexes.

Diamonds with Fancy black color grades can have either natural or treated color origin. *Natural* black diamonds are usually colored by inclusions of sulfides, graphite, magnetite, hematite, or iron-bearing inclusions (e.g., Titkov et al., 2003). A rare natural diamond (of undisclosed geographic origin) colored by abundant brown radiation stains has previously been examined by GIA's Carlsbad laboratory (Ardon, 2013). *Treated* black diamonds are often those that are heavily fractured naturally and then treated at low-pressure and high-temperature (LPHT) conditions to graphitize the fractures and turn them black (Hall and Moses, 2001; Notari, 2002). Artificial irradiation can also produce dark colors that appear black (Collins, 1982; Kitawaki, 2007).

The Marange locality in eastern Zimbabwe is well known for producing diamonds that contain both octahedral and cuboid sectors (mixed-habit diamonds) where the cuboid sectors are visible to the eye due to abundant micro-inclusions of graphite (Rakovan et al., 2014; Smit et al., 2016). These micro-inclusions, informally known in the gem trade as "clouds," give the diamonds a brown-gray appearance that lowers their value. Heat treatment of these lower-quality graphite-containing Marange diamonds has the potential to introduce gem-quality treated black diamonds into the market. In natural diamonds, these graphite micro-inclusions are around 1 µm in diameter; during heating above 1200°C, they become larger. After annealing at 1700°C, the grain size increases to 11–16 µm, causing the cuboid sectors to appear opaque black (Eaton-Magaña et al., 2017). The challenge for gem laboratories is to confidently distinguish these treated black diamonds from naturally occurring black diamonds.

Here our goal was to document a suite of untreated Marange diamonds, all with Fancy Dark brown to Fancy black GIA color grades, so that their characteristics could be distinguished from any suspected treated black diamonds. When viewing the samples, however, it became clear that the appearance of the these dark Marange diamonds was due not only to graphite clouds but also to abundant graphite needles and dark brown radiation stains occurring within surface-reaching fractures.

See end of article for About the Authors and Acknowledgments.
Gems & Gemology, Vol. 54, No. 2, pp. 132–148,
http://dx.doi.org/10.5741/GEMS.54.2.132

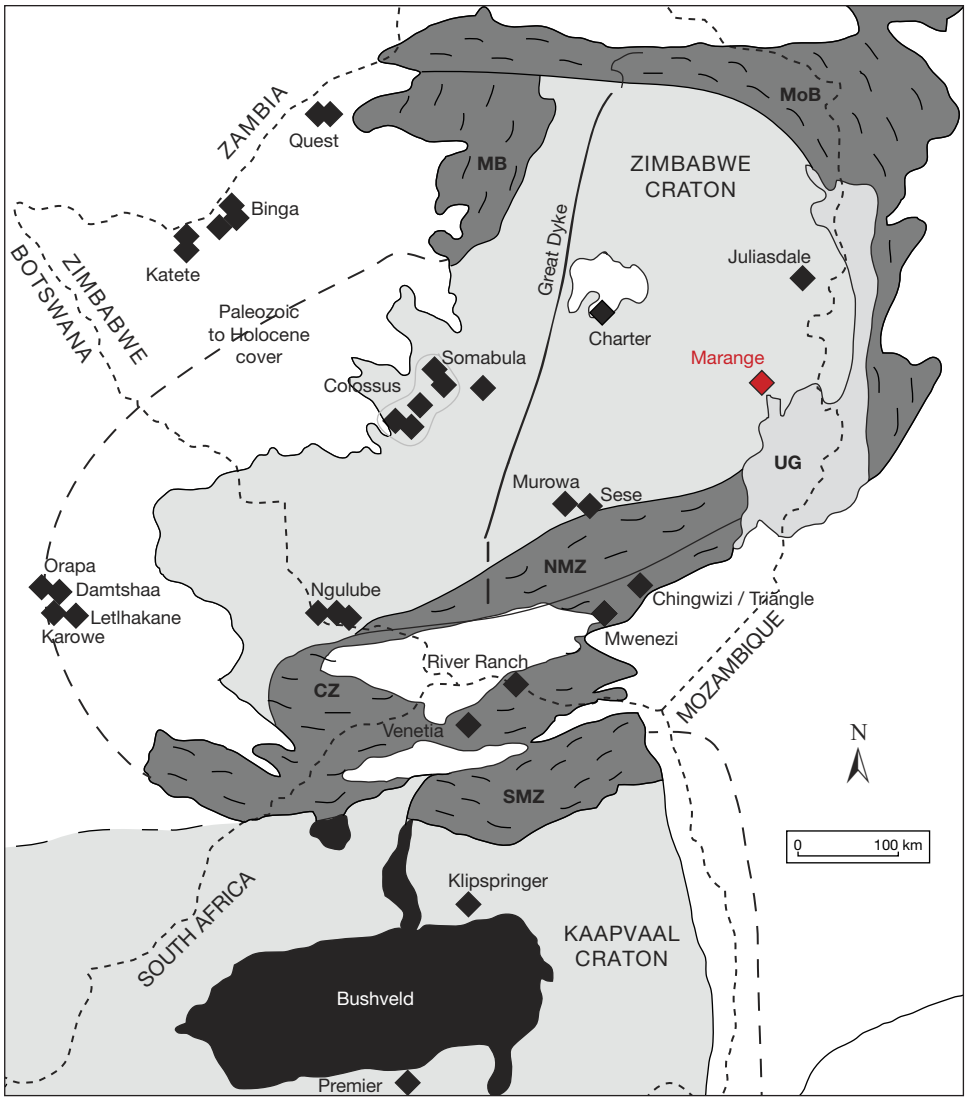

Figure 1. Geological map of Zimbabwe, northern South Africa, and eastern Botswana that shows the Kaapvaal and Zimbabwe cratons and their bounding mobile belts. Image taken from Smit et al. (2016), which is adapted from Hanson et al. (2011) and McCourt et al. (2004). Kimberlite localities (indicated here as diamonds) from Moore et al. (2009) and Google Maps. Marange alluvial diamonds occur in eastern Zimbabwe in sediments that were reworked from the basal conglomerate of the ~1.1 Ga Umkondo Group (UG; Hanson et al., 2004; Moore et al., 2009, and references therein). The 2.7–2.6 Ga Limpopo Belt is divided into the CZ (Central Zone), NMZ (Northern Marginal Zone), and SMZ (Southern Marginal Zone). MB is the 2.1–1.8 Ga Magondi Belt (Stowe, 1989; Jacobs et al., 2008), and MoB is the 0.55 Ga Mozambique Belt.

MARANGE ALLUVIAL DIAMOND LOCALITY

Primary diamond deposits are always found in association with extremely old portions of the earth's crust known as cratons (e.g., Clifford, 1966). The combined Kaapvaal and Zimbabwe cratons in Botswana, South Africa, and Zimbabwe host many of the world's famous diamond mines. For example, the Kimberley mines on the southwestern Kaapvaal craton are famous as the type locality for kimberlite, the primary source rock for diamonds. Also, the Karowe mine in central Botswana is an exciting new source for super-large colorless diamonds near the western margin of the Zimbabwe craton (www.lucaradiamond.com).

The Marange alluvial diamonds occur on the Zimbabwe craton near the Zimbabwe-Mozambique border. The Zimbabwe craton comprises 3.6 to 3.5 Ga basement granite-greenstone terranes (Wilson, 1990, and references therein), although an older Paleoarchean heritage is suggested by ~3.9 Ga detrital zircons (Dodson et al., 1988; Zeh et al., 2014) and 3.97 to 3.75 Ga chromites from ultramafic intrusions (Nägler et al., 1997). The Zimbabwe craton amalgamated with the Kaapvaal craton to the south, through successive terrane accretions that included the Central Zone of the Limpopo Mobile Belt between 2.70 and 2.61 Ga (figure 1; Zeh et al., 2009, 2013).

The Marange diamonds were discovered by De Beers in 2001 in >1.1 Ga Umkondo Group conglomerates near the eastern edge of the Zimbabwe craton (figure 1; Hanson et al., 2004; Moore et al., 2009). These conglomerates were deposited into the Umkondo Foreland Basin, through fluvial erosion of diamondiferous kimberlites in the more westerly

Figure 2. Rough Marange diamonds previously examined at GIA. These are not the same rough from which the black diamonds in this study were cut, but are shown as examples of typical rough Marange diamond morphologies. These diamonds are generally large (5–7 ct each), with resorbed morphologies and non-transparent coatings. Rather than arising from fibrous growth, these coatings are thought to be the result of radiation damage combined with metamorphic heating (Moore et al., 2009, and references therein). Photos by Wuyi Wang.

parts of the Zimbabwe craton, and have been locally weathered to much softer Quaternary sediments (Moore et al., 2009). The primary source kimberlites for the Marange diamonds have not been found and, due to a lack of studies focusing on mineral inclusions from these diamonds, their age and source paragenesis (eclogitic vs. peridotitic) is unknown.

Diamonds from Marange first entered the market in 2006, and early artisanal mining focused on the softer Quaternary sediments. Mining has since been mechanized, and several mining companies have operated in the Marange fields—including Anjin Investments, Diamond Mining Company, Gye Nyame Resources, Jinan Mining, Kusena Diamonds, Marange Resources, and Mbada Diamonds. In 2016, many of these operations were acquired by the government-controlled Zimbabwe Consolidated Diamond Company (ZCDC).

Marange diamonds are typically large (5–7 ct apiece; figure 2) and abundant (with grades ranging between 1 and >30 carats per ton), which means they were discovered *in situ* in the conglomerate during exploration field work (M. de Wit, pers. comm., 2016). A unique characteristic of Marange diamonds is their thin, non-transparent coating (figure 2). Rather than arising from fibrous growth, this coating is thought to be the result of radiation damage combined with metamorphic heating (Moore et al., 2009, and references therein).

METHODS

Optical Absorption Spectroscopy. Optical absorption spectra were collected using an Ocean Optics HR4000 spectrometer equipped with a charge-coupled device (CCD) array, a 10 μm entrance slit, and 300 lines/mm grating. The resulting spectral resolution is 1.4 nm. Spectra were collected between 380 and 980 nm while the diamonds were cooled to liquid nitrogen temperatures (77 K). Integration time for each spectrum was 0.5 seconds with 30 accumulations.

Fourier-Transform Infrared (FTIR) Spectroscopy. FTIR absorption spectra were collected over the 400–6000 cm^{-1} range using a Thermo Nicolet Nexus 6700 spectrometer furnished with KBr and quartz beam splitters and a diffuse-reflectance infrared Fourier-transform (DRIFT) accessory. Spectra were collected with a resolution of 1 cm^{-1} and over 32 scans. During analyses, the instrument and sample chambers were

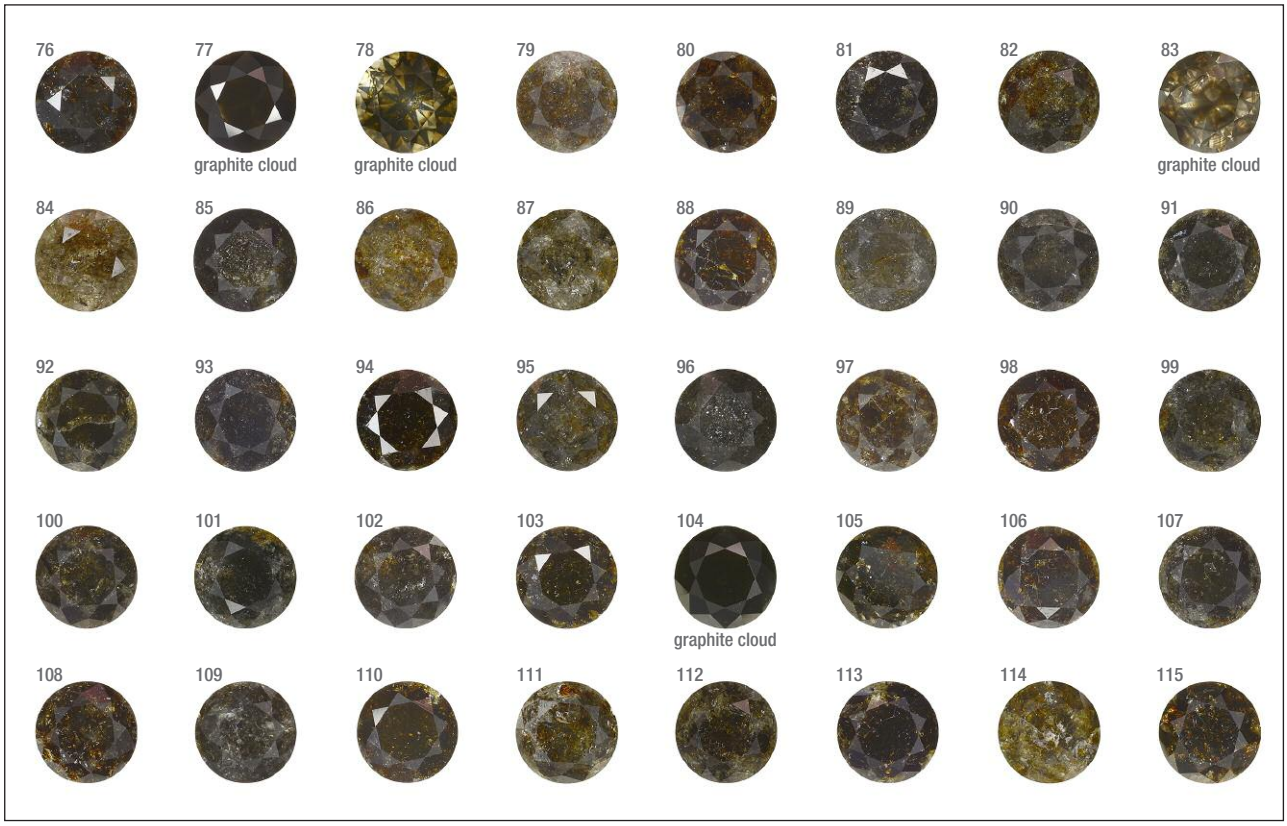

Figure 3. Table-up images of the 40 natural Fancy Dark brown to Fancy black Marange diamonds from this study. The diamonds range between 0.39 and 3.11 ct, and between 4.47 and 8.75 mm in diameter (see table 1). All the diamonds have a dark appearance due to graphite needles and abundant radiation stains, except for four with dark clouds comprised of micron-sized inclusions of graphite. Photos by Jian Xin (Jae) Liao.

continuously purged with dry air to minimize atmospheric contamination.

DiamondView Imaging. Images of the internal growth zoning were obtained using an International Institute of Diamond Grading and Research (IIDGR) DiamondView instrument, which uses broadband ultraviolet radiation (filtered for $\lambda < 230$ nm) to induce luminescence in diamond (Welbourn et al., 1996). Integration time, aperture size, and gain settings were all adjusted between samples to obtain optimal brightness and contrast for each image.

Photoluminescence (PL) Spectroscopy. Photoluminescence spectra were collected using a Renishaw InVia Raman confocal microspectrometer equipped with a CCD detector. PL spectra were taken using three different laser excitation wavelengths: 488 nm (Ar-ion laser), 632.8 nm (He-Ne laser), and 830 nm (diode laser). All diamonds were cooled to 77 K by direct immersion in liquid nitrogen to improve the intensity and sharpness of any observed peaks. Spectra were recorded over the ranges of 490 to 650 nm (488 nm excitation), 635 to 850 nm (632.8 nm excitation), and 837 to 1000 nm (830 nm excitation). Integration times for all spectra were 10 seconds, with 1 accumulation. Spectra were collected on a RenCam air-cooled CCD detector after passing through a spectrometer using an 1800 lines/mm grating (488 and 633 nm excitation) and a 1200 lines/mm grating (830 nm excitation).

RESULTS

Sample Characteristics. This study is based on 40 natural round brilliant diamonds from the Marange mining operations in Zimbabwe (figure 3). The diamonds all received Fancy Dark brown to Fancy black color grades from GIA, and they ranged between 0.39 and 3.11 ct (table 1). These samples were obtained from the trade and had undergone no heat or irradiation treatments. The overwhelming majority (36 out of 40 samples) were heavily fractured and contained numerous dark graphitic needle-like inclusions. These diamonds had various degrees of brown radiation stains that were localized along the surface-

TABLE 1. Physical and spectroscopic characteristics of the 40 natural brown-black Marange diamonds analyzed in this study.

Sample no.	Dimensions (mm)	Weight (carat)	GIA color grade	3050 cm^{-1} CH_4 peak in FTIR	GR1 in optical absorption	GR1 in 633 nm PL	H3 in 488 nm PL	H2 in 830 nm PL	700.5 Ni peak in 633 nm PL	926 nm Ni peak in 830 nm PL
76	4.47–4.49 × 3.03	0.39	Fancy black	×					×	×
77	5.99–6.00 × 3.69	0.83	Fancy black	×					×	×
78	5.96–5.97 × 3.71	0.85	Fancy Dark brown	×			×	×	×	×
79	6.15–6.17 × 4.03	0.99	Fancy black			×	×		×	×
80	6.06–6.08 × 4.17	1.00	Fancy black				×	×		×
81	6.18–6.20 × 4.02	1.00	Fancy black			×	×		×	×
82	6.24–6.27 × 4.01	1.00	Fancy black	×		×	×		×	×
83	6.13–6.16 × 4.12	1.01	Fancy Dark brown	×			×		×	×
84	6.31–6.36 × 4.17	1.09	Fancy Dark brown		×	×	×	×	×	×
85	6.10–6.13 × 4.06	1.03	Fancy black				×		×	×
86	6.14–6.17 × 4.14	1.03	Fancy Dark brown		×	×	×	×	×	×
87	6.23–6.26 × 4.11	1.03	Fancy Dark gray	×			×	×	×	×
88	6.06–6.10 × 4.19	1.05	Fancy black		×	×	×			×
89	6.46–6.50 × 4.06	1.06	Fancy black	×			×		×	×
90	6.32–6.34 × 4.16	1.06	Fancy black	×			×		×	×
91	6.34–6.37 × 4.04	1.06	Fancy black	×					×	×
92	6.32–6.34 × 4.08	1.07	Fancy black						×	×
93	6.55–6.58 × 4.07	1.10	Fancy black				×		×	×
94	6.53–6.54 × 3.98	1.09	Fancy black		×	×	×			×
95	6.35–6.42 × 4.08	1.09	Fancy black	×			×		×	×
96	6.32–6.33 × 4.25	1.10	Fancy black	×			×		×	×
97	6.43–6.46 × 4.07	1.12	Fancy black			×	×	×	×	×
98	6.41–6.45 × 4.10	1.11	Fancy black		×	×	×	×		×
99	6.25–6.26 × 4.29	1.12	Fancy black	×	×	×	×		×	×
100	6.33–6.36 × 4.28	1.12	Fancy black	×	×	×	×		×	×
101	6.41–6.42 × 4.27	1.14	Fancy black				×		×	×
102	6.35–6.41 × 4.26	1.14	Fancy black	×			×		×	×
103	6.58–6.60 × 4.28	1.18	Fancy black		×	×	×			×
104	6.51–6.55 × 4.29	1.19	Fancy black	×					×	×
105	6.62–6.64 × 4.40	1.27	Fancy black		×	×	×		×	×
106	6.58–6.62 × 4.27	1.26	Fancy black		×	×	×		×	×
107	6.46–6.49 × 4.50	1.27	Fancy black	×			×		×	×
108	6.67–6.68 × 4.55	1.34	Fancy black		×		×		×	×
109	6.72–6.73 × 4.53	1.35	Fancy black				×		×	×
110	7.16–7.21 × 4.26	1.44	Fancy black		×	×	×		×	×
111	7.02–7.03 × 4.57	1.50	Fancy black	×	×	×	×		×	×
112	7.00–7.04 × 4.70	1.52	Fancy black		×	×	×		×	×
113	7.45–7.48 × 4.62	1.71	Fancy black		×	×	×			×
114	8.20–8.26 × 5.21	2.24	Fancy black		×	×	×		×	×
115	8.71–8.75 × 6.07	3.11	Fancy black		×	×	×	×		×
			Number		17	20	35	8	33	40
			Percentage		42.5	50	87.5	20	82.5	100

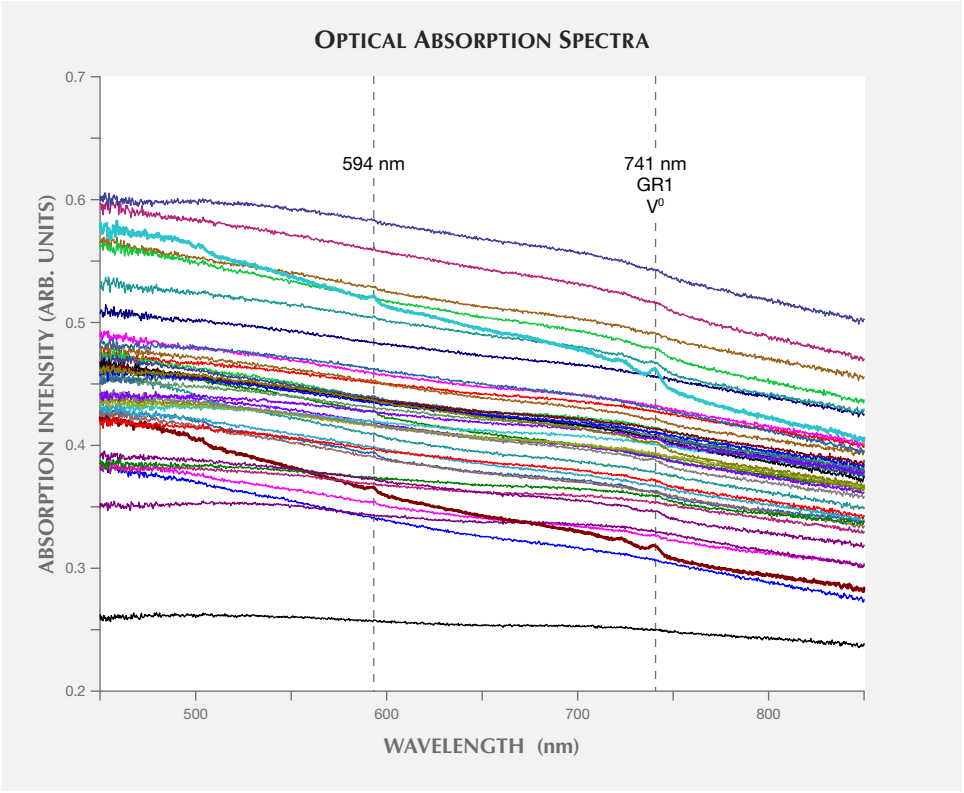

Figure 4. Optical absorption spectra (77 K) of all the samples in the suite. Weak GR1 (V^0 at 741 nm) was observed in 43% of the samples. Two samples with the highest-intensity GR1 are 84 (maroon spectrum) and 114 (teal spectrum). GR1 was accompanied by the 594 nm peak associated with annealing after irradiation (Collins et al., 1986). All samples have an absorption continuum with an increasing slope toward the ultraviolet. This may be intrinsic in part and due to vacancy clusters, but analytical artifacts cannot be ruled out (see text for further details).

reaching fractures. The original bodycolor of the diamonds was obscured by the presence of fractures, dark inclusions, and radiation stains. Four samples (77, 78, 83, and 104; see figure 3) were not heavily fractured and instead contained clouds of dark pinpoint (or micro-) inclusions.

Origin of Dark Appearance and Color. Any defects that are present in the visible spectrum (390 to 700 nm) and in sufficient concentration to be detected by optical absorption spectroscopy can influence the bodycolor of a diamond.

The optical absorption spectra for all the samples had a slight absorption continuum with an increasing slope toward the ultraviolet (figure 4). Brown diamonds typically have such an absorption slope, which is attributed to vacancy clusters formed along deformation lamellae (Fisher et al., 2009). However, the spectra for this study were obtained on faceted diamonds, and the instrument's integrating sphere made accurate baseline subtraction a challenge. This means that while we cannot discount that there may be an intrinsic absorption continuum in some samples, any observed slope may also be an analytical artifact.

Very weak GR1 (741 nm) was visible in 17 out of the 40 diamonds (43%) (figure 4). The two diamonds with the highest-intensity GR1 in optical absorption were samples 84 and 114 (maroon and teal in figure 4). GR1 is the neutral vacancy defect (V^0), produced during both natural and artificial irradiation (Clark et al., 1956). Where GR1 is present in the optical absorption spectra, the 594 nm peak is also seen (figure 4), indicating that natural annealing and associated vacancy migration occurred (Collins et al., 1986). These features are most likely related to the brown radiation stains visible on the surface of the diamonds. Typically, these stains do not penetrate deep into the diamond (<30 µm; see Crookes, 1904; Wagner, 1914; Lind and Barwell, 1923). With optical absorption spec-

In Brief

- The Marange alluvial deposits in Zimbabwe produce many naturally irradiated diamonds.
- The abundance of brown radiation stains combined with the intense fracturing impart a dark bodycolor to the diamond.
- Some Marange diamonds are colored by "clouds" of graphite micro-inclusions that are restricted to cuboid growth sectors.

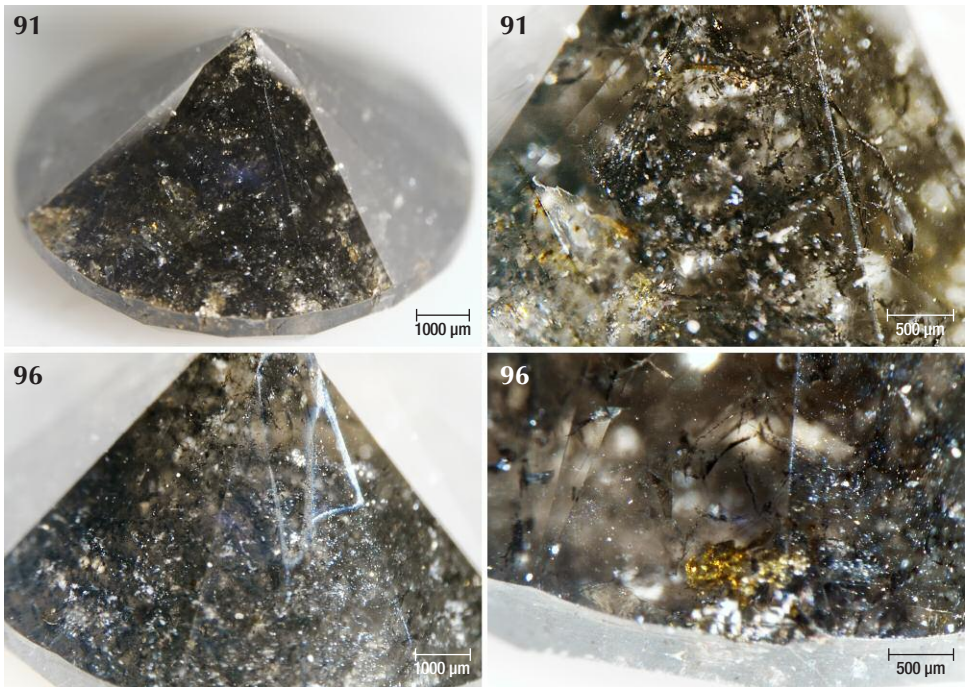

Figure 5. The appearance of these two diamonds is dominated by black graphitic needles, with very few brown radiation stains. These graphite needles are all significantly larger than the micron-sized graphite inclusions forming the dark clouds in figure 9. Photos by Karen Smit.

troscopy, the entire thickness of the diamond is sampled, so the signal from irradiation-related defects is diluted. This may explain why the peak intensities of GR1 and 594 nm are low, whereas there are abundant radiation spots visible on the surface and along fractures. The dark appearance of the diamonds is therefore related to the combined presence of dark mineral inclusions and abundant brown radiation stains.

The majority of samples were colored by graphite needles (figure 5) along with brown radiation stains occurring along surface-reaching internal fractures (figures 6 and 7). Marange diamonds have previously

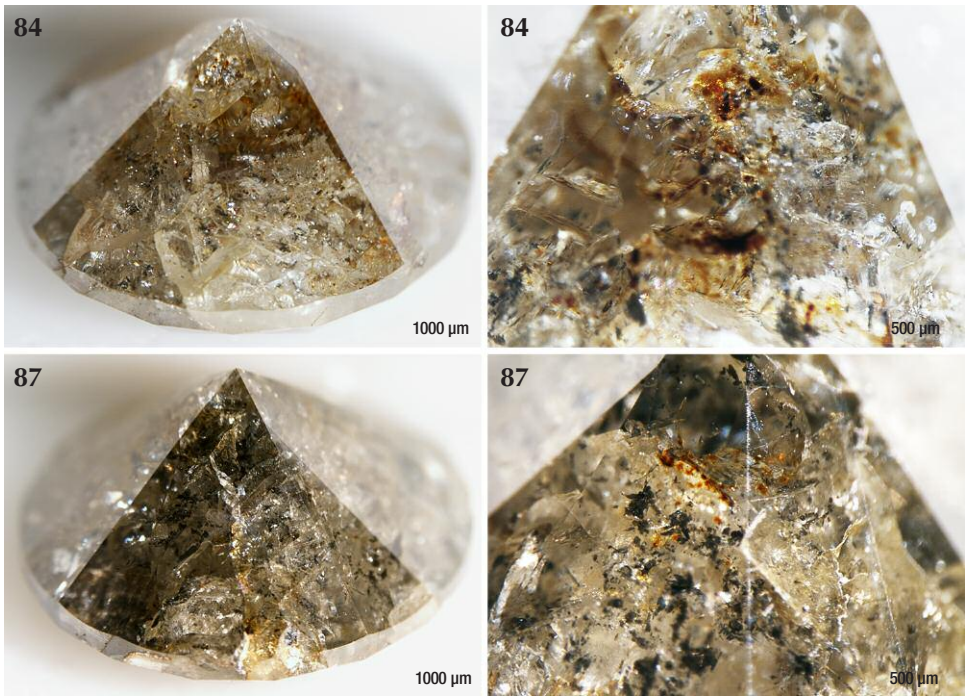

Figure 6. Images of two diamonds that are only lightly colored by brown radiation stains along internal fractures, but also contain abundant graphite needles. These graphite needles are all significantly larger than the micron-sized graphite inclusions forming the dark clouds in figure 9. Photos by Karen Smit.

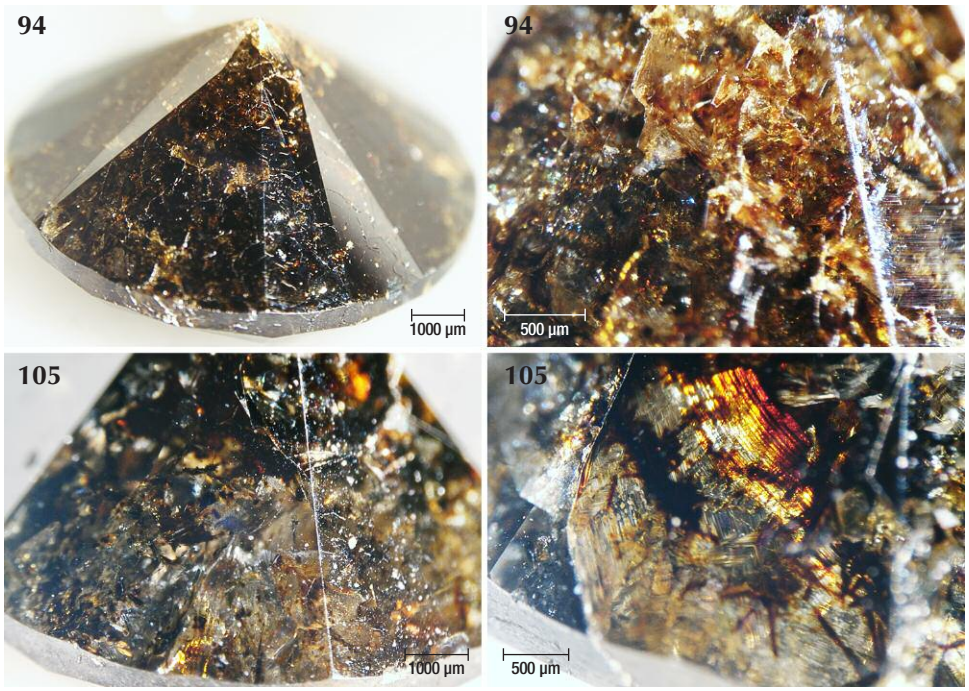

Figure 7. These two diamonds have the darkest appearance due to abundant brown radiation stains, combined with graphite needles. These graphite needles are all significantly larger than the micron-sized graphite inclusions forming the dark gray to black clouds in figure 9. Photos by Karen Smit.

been described with both green and brown radiation stains (Breeding and Wang, 2014; Eaton-Magaña et al., 2017; and unpublished GIA data). In all 40 samples described for this study, however, only brown radiation stains were observed (figure 8).

Four of the diamonds were not colored by graphite needles or brown radiation stains. Instead, their dark appearance was due to clouds of graphitic micro-inclusions (figures 3 and 9), similar to Marange diamond samples described in Smit et al. (2016) and Eaton-Magaña et al. (2017). These clouds appear to correlate with growth zones within the diamonds (figures 9 and 10). These four samples did appear to have a brown bodycolor that might have been due to the absorption continuum seen in the optical absorption spectra (again, see figure 4) and was likely related to vacancy clusters formed in the diamond lattice through deformation (Fisher et al., 2009).

Nitrogen and Other Defects Observed in FTIR Spectra. Due to high amounts of nitrogen, the nitrogen concentration and nitrogen aggregation characteristics of the Marange diamonds in this study could not be

Figure 8. Individual brown radiation stains visible within fractures. This feature is most consistent with natural radioactive fluids infiltrating the diamond along the fractures, and it would not be produced by artificial irradiation. Photos by Karen Smit.

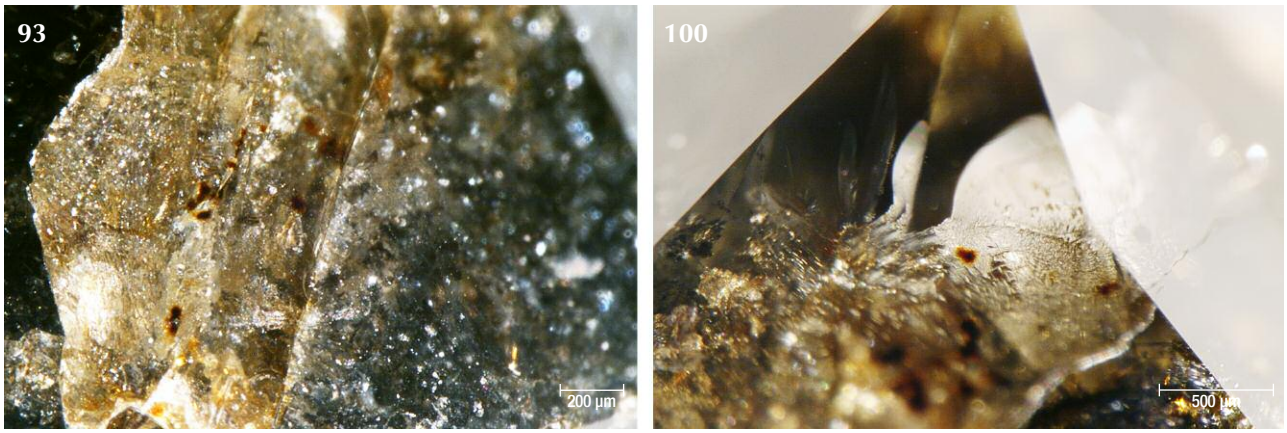

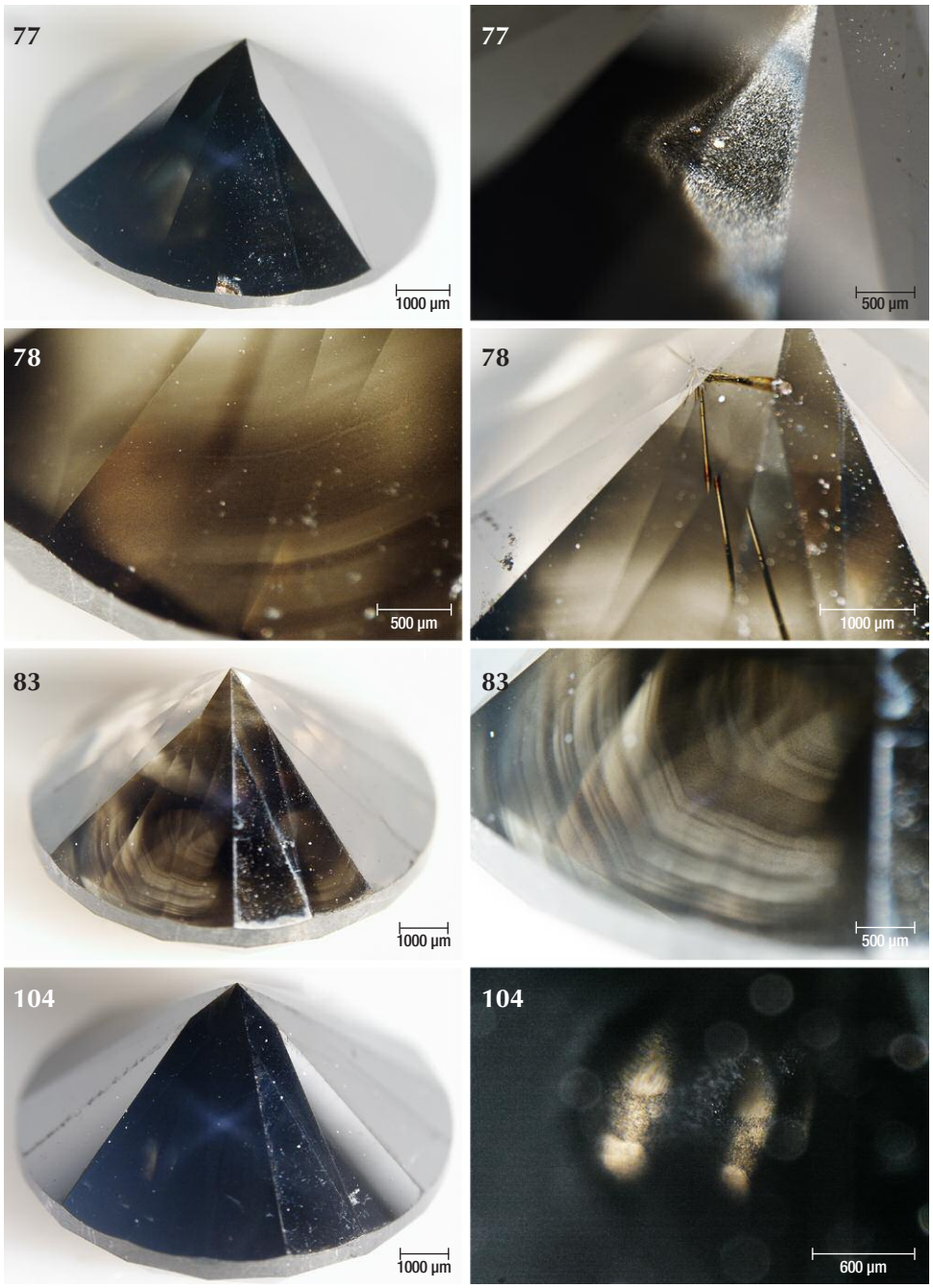

Figure 9. Images of the four diamonds that contain clouds of micron-sized inclusions of graphite that impart a dark appearance to the diamonds. Graphite in Marange diamonds has previously been found to occur in association with methane fluid inclusions (Smit et al., 2016). Also visible in sample 78 are radiation stains along the fractures in the diamond. Photos by Karen Smit.

quantified. Previously, FTIR mapping across thin (0.5 mm) Marange diamond plates has allowed for quantification of nitrogen in the one phonon region. Smit et al. (2016) reported FTIR-determined nitrogen concentrations between 971 ppma and 2628 ppma, all with less than 30% of nitrogen occurring as B centers (N_4V, where V is a vacancy). All 40 diamonds in this current study had strong VN_3H peaks (Goss et al., 2014) at 3107 cm^{-1} (stretching mode) and 1405 cm^{-1} (bending mode), as well as many other hydrogen-related defects in the 3050–3311 cm^{-1} region (figure 11). A small 3050 cm^{-1} peak seen in 17 of the 40 diamonds (42.5%) is indicative of methane (Benedetti et al., 1999; Teinturier et al., 2002; see figure 11).

Previous studies have noted the spatial association of methane and graphite micro-inclusions exclusively in the cuboid sectors of Marange diamonds (e.g., Smit et al., 2016). All diamonds in this study that contain methane peaks in FTIR also contain graphitic micro-inclusions (figure 9 and table 1). Based on our previous

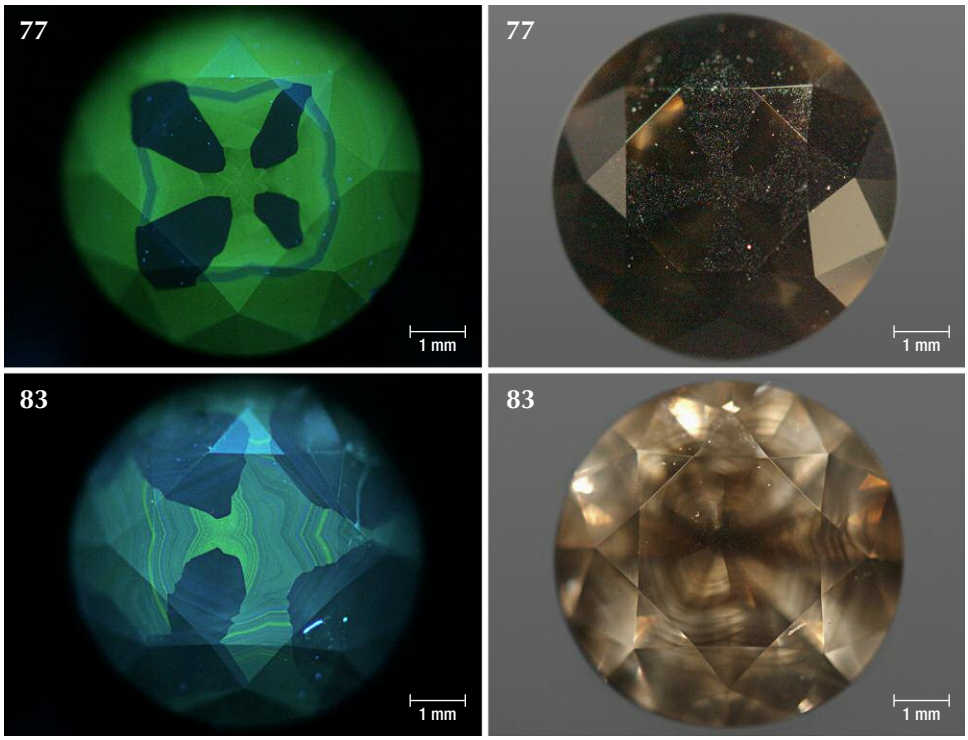

Figure 10. DiamondView and visible-light images of two diamonds that are colored exclusively by clouds comprised of micron-sized inclusions of graphite (causing the dark appearance). These diamonds display cuboctahedral growth, with graphite micro-inclusions (clouds) that occur only within the cuboid sectors. Graphite in Marange diamonds is associated with methane fluid inclusions (Smit et al., 2016) as well as Ni-N defects that luminesce a green-yellow color with UV excitation (Rondeau et al., 2004; Lang et al., 2004; Howell et al., 2013; Rakovan et al., 2014). Photos and images by Karen Smit.

work on Marange diamonds, graphite is reasonably assumed to occur in the cuboid sectors. Additionally, high nitrogen contents, the presence of methane, and the other hydrogen-related FTIR features are all consistent with previously described Marange diamonds (Smit et al., 2016; Eaton-Magaña et al., 2017).

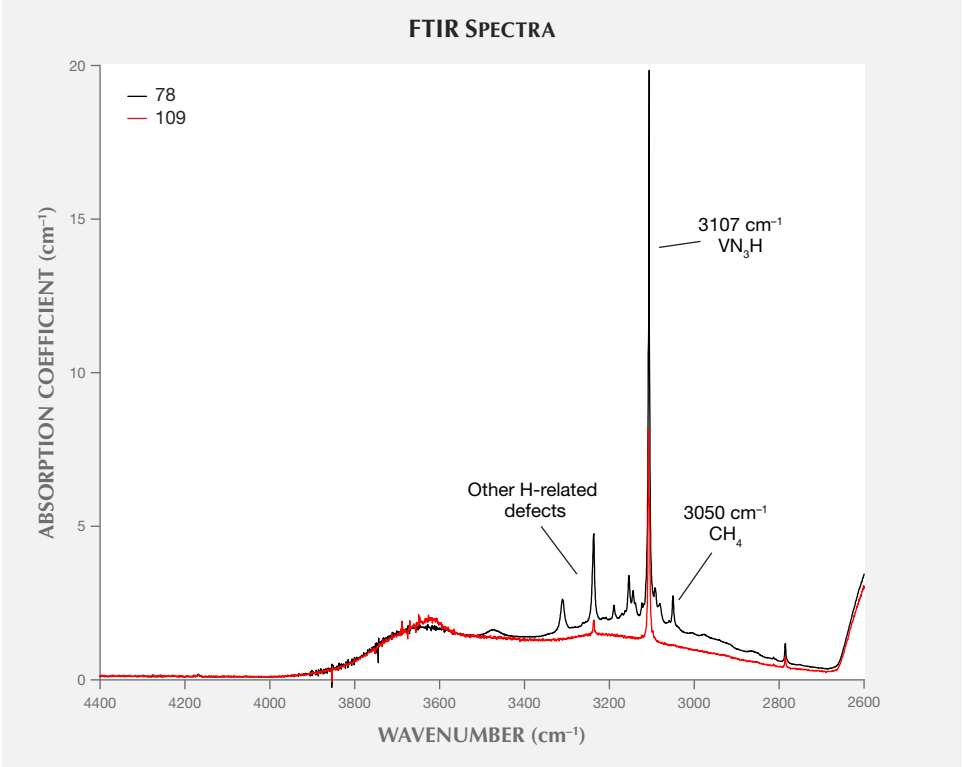

Figure 11. FTIR spectra for two representative samples that show the presence and absence of CH_4 at 3050 cm^{-1}. The sample containing CH_4 also shows other hydrogen-related peaks in the vicinity of the VN_3H peak at 3107 cm^{-1} (Goss et al., 2014). Previous work on other Marange diamonds showed that CH_4 inclusions are restricted to cuboid sectors and closely associated with the clouds of graphitic micro-inclusions (Smit et al., 2016).

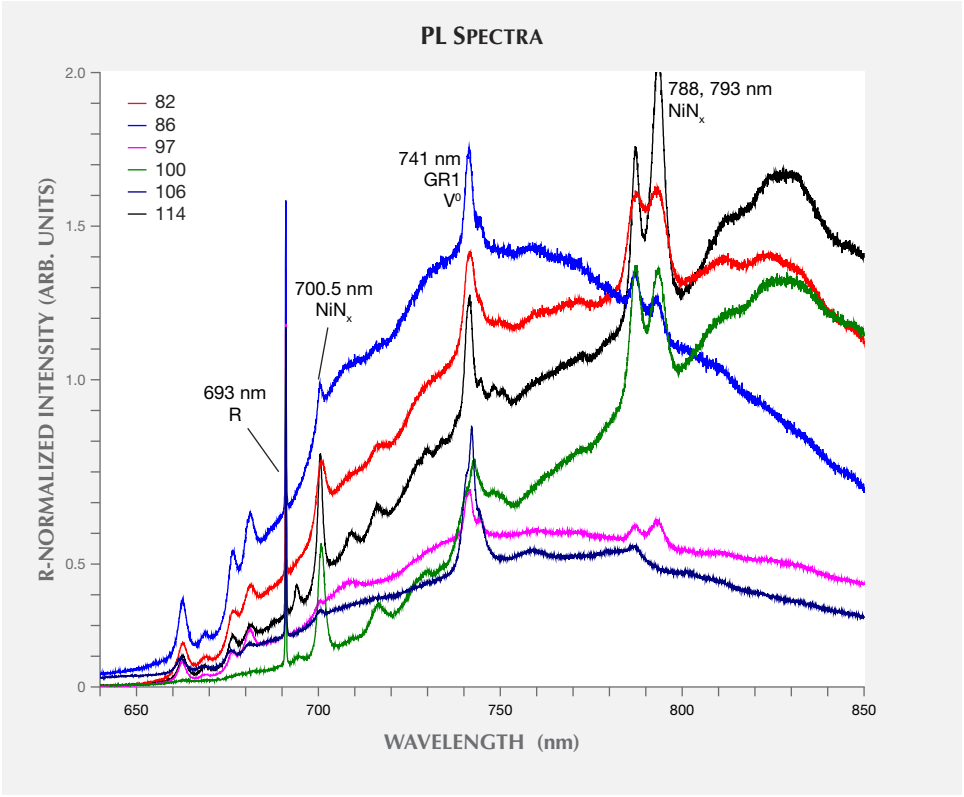

Figure 12. PL spectra (77 K) taken with a 633 nm laser excitation source. In all spectra, the diamond Raman peak (R) is normalized to an intensity of 1 so that the intensities of PL peaks in different samples are comparable. GR1 (741 nm) is observed in 50% of the 633 nm PL spectra compared to 43% of optical absorption spectra, due to the enhanced sensitivity of the PL technique. Also shown are peaks related to NiN_x at 700.5, 788, and 793 nm.

Defects Observed in PL Spectra. Defects that are only detectable by PL spectroscopy and not present in sufficient quantities to be detected through optical absorption spectroscopy have no influence on the bodycolor of diamonds. Nevertheless, these defects can provide important information on the diamonds' geological history.

Nickel-Related Defects. Nickel-related defects were observed in all 40 samples in this suite (again, see table 1). Previous studies of Marange and other mixed-habit diamonds have shown that these Ni-related defects only occur in the cuboid sectors (Lang et al., 2004; Rondeau et al., 2004; Howell et al., 2013; Smit et al., 2016). In this study, PL spectra were collected randomly, and as such are representative of the bulk diamond, so sector-dependent Ni incorporation was not evaluated. However, the observation of Ni-related defects in all 40 samples suggests at least some cuboid growth in all of the samples. Peaks at 700.5, 788, and 793 nm (observed using 633 nm laser excitation) as well as 926 nm (830 nm laser excitation) relate to NiN_x complexes that can form during high-temperature annealing (Iakoubvskii and Adriaenssens, 2002; Hainschwang et al., 2005; Yelisseyev and Kanda, 2007; Dischler, 2012; see figures 12 and 13). These NiN_x complexes (where x = 1–4) have a basic structure as Ni^+ in a divacancy interstitial position with six carbon neighbors (NE4 EPR center correlating with 1.4 eV/883 nm optical center; Nazaré et al., 1991; Collins, 2000; Lang et al., 2004). When N substitutes for the carbon atoms that surround Ni, the NE1–NE8 EPR centers are created (e.g., NE1 = NiN_2 and NE8 = NiN_4; Nadolinny et al., 1999; Johnston and Mainwood, 2003).

Defects Related to Irradiation and Annealing. Since PL spectroscopy is more sensitive than optical absorption spectroscopy, GR1 (V^0) was observed in 50% of the 633 nm PL spectra compared to 43% of the optical absorption spectra (figure 12 and table 1). H3—NVN^0 at 503.2 nm—occurred in 35 out of the 40 Marange diamonds we analyzed for this study (figure 14). H3 can form through high-temperature annealing of diamonds and forms when vacancies migrate through the diamond lattice and become trapped at A centers (N pairs). H2 is the negative charge state of H3—NVN^- at 986 nm—and can form by accepting an electron from isolated substitutional nitrogen (N_S^0). Weak H2 was observed in only eight diamonds in this suite (20%; see figure 13 and table 1). Although Marange diamonds are type IaAB and do not have sufficient N_S^0 to be detected through FTIR spectroscopy, natural diamonds are known to contain trace amounts of N_S^0 that could contribute to H2 for-

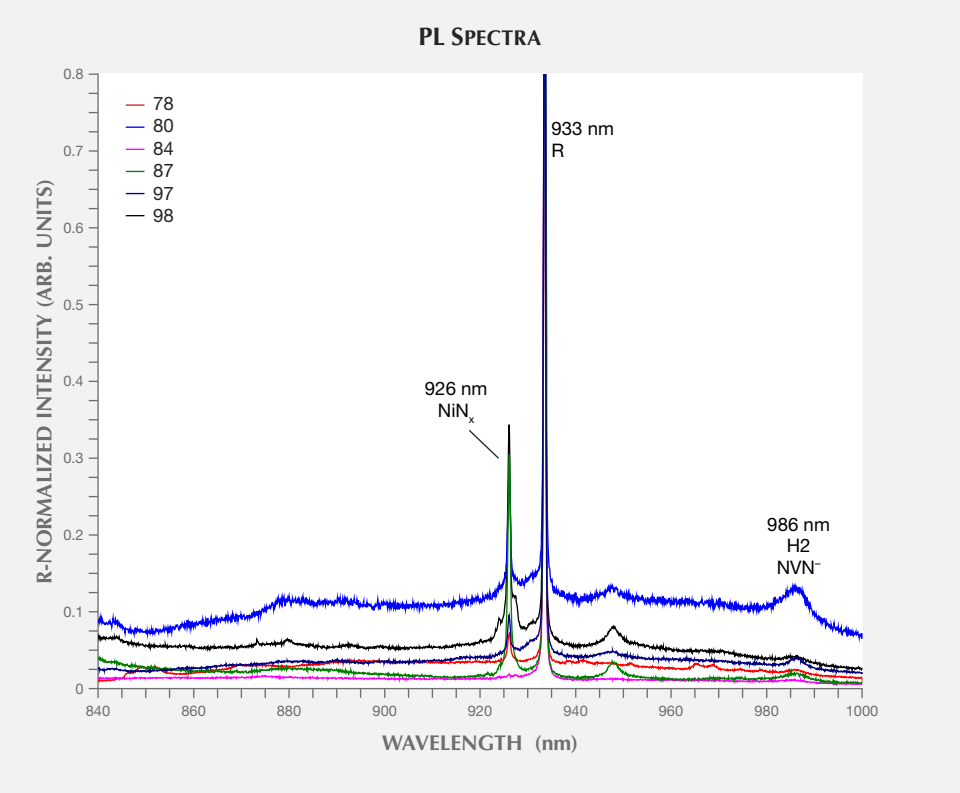

Figure 13. PL spectra (77 K) taken with an 830 nm laser excitation source show the 926 nm peak related to NiN_x defects and H2 at 986 nm. In all spectra, the diamond Raman peak (R) is normalized to an intensity of 1 so that the intensities of PL peaks in different samples are comparable.

mation (e.g., type IaB diamonds contain 4 ± 2.5 ppb N_S^0 detected through EPR spectroscopy (Newton, 2011). For comparison, the detection limit in FTIR spectroscopy is typically around 1 ppma.

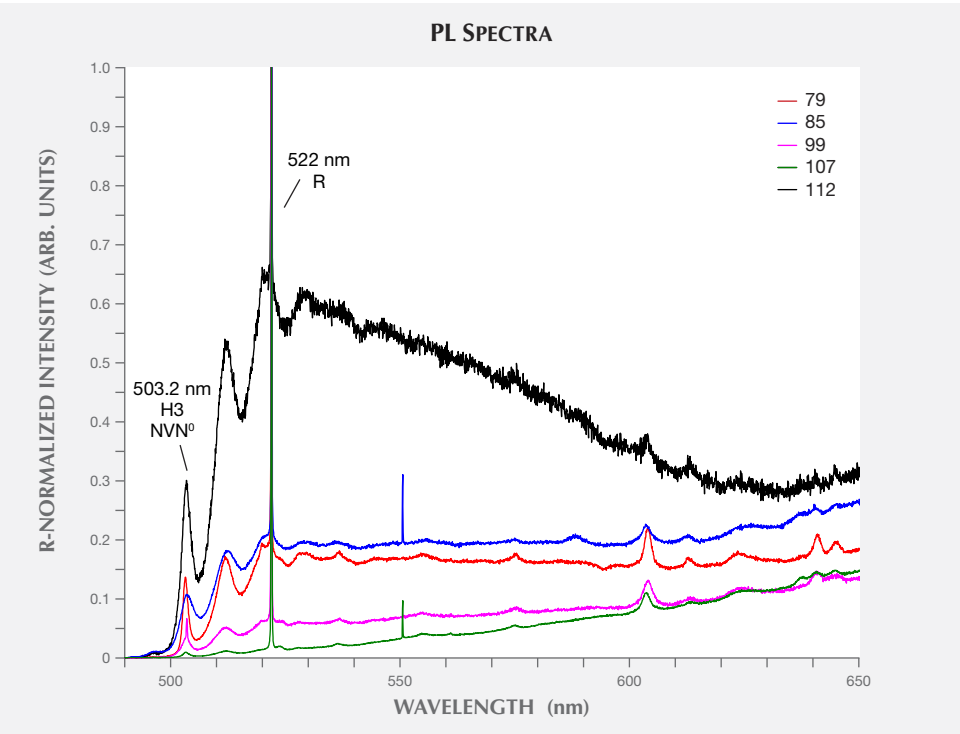

Figure 14. PL spectra (77 K) taken with a 488 nm laser excitation source, with the zero phonon line (ZPL) of H3 observed at 503 nm, along with its vibronic structure up to around 520 nm. In all spectra, the diamond Raman peak (R) is normalized to an intensity of 1 so that the intensities of PL peaks in different samples are comparable. The sharp line visible at around 550 nm in two samples is from the liquid nitrogen used to cool the diamonds.

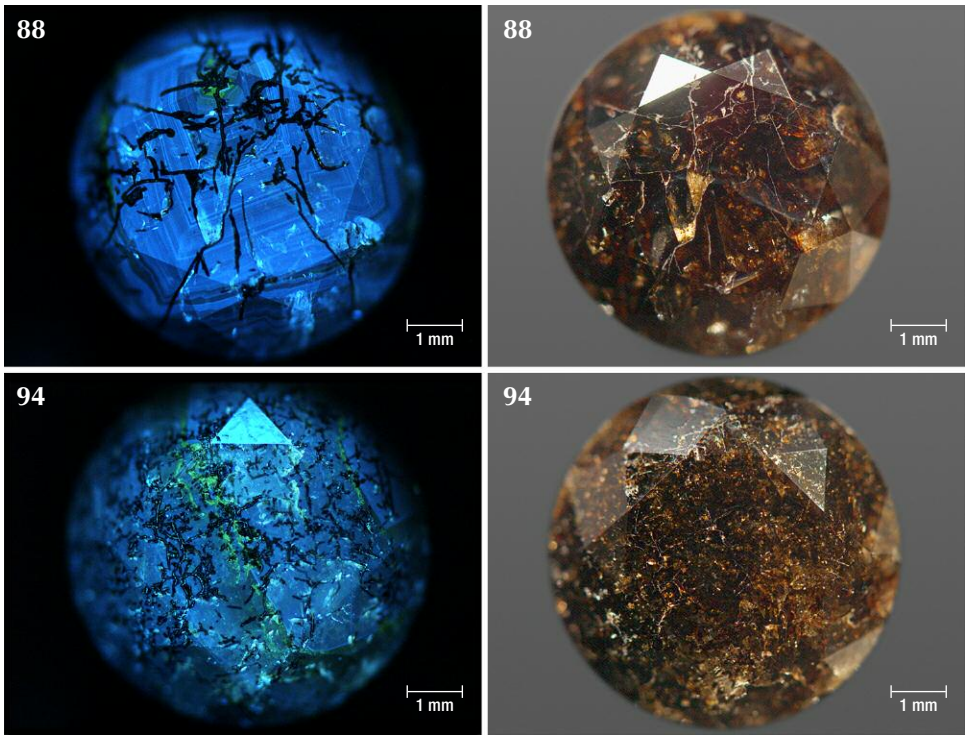

Figure 15. DiamondView and visible light images of two diamonds that show radiation stains within fractures in the diamond. Non-luminescent regions in the DiamondView images are associated with extensive radiation damage along fractures in the diamonds. Photos and images by Karen Smit.

Features Observed in DiamondView Images. The DiamondView uses a UV source to excite luminescent defects in the diamond lattice. Similar to cathodoluminescence, growth zones within diamond are visible if they contain different concentrations of defects that may produce different color responses. DiamondView images of the Marange diamonds are dominated by blue and yellowish green luminescence, where blue luminescence can be related to both "Band A" and/or the N3 (VN_3) center (van Wyk, 1982; Collins, 1992; Welbourn et al., 1996) and the yellowish green luminescence could be due to H3 (NVN^0) and/or the NiN-related defects observed in PL spectra (e.g., Welbourn et al., 1989, 1996).

Cuboctahedral (mixed-habit) growth sectors were visible in some samples and most obvious in the diamonds colored exclusively by clouds of graphitic micro-inclusions (figures 9 and 10). Following observations on a different suite of Marange diamonds, as well as mixed-habit diamonds from other localities (Lang et al., 2004; Rondeau et al., 2004; Howell et al., 2013), cuboid sectors always contain the graphite clouds and Ni-related defects, whereas the octahedral sectors are free of any inclusions and Ni-related defects (Smit et al., 2016). Based on the close spatial association of graphite and methane in other Marange diamonds, the cuboid sectors containing graphite clouds in this study can also reasonably be expected to contain methane (as identified through bulk FTIR analyses; figure 11).

Areas of irradiation damage on the Marange diamonds showed no luminescence and appeared darker than the bulk of the stone (figure 15), features that were also observed in diamonds from the Grib mine (Arkhangelsk region, Baltic shield; Rubanova et al., 2009). These non-luminescent areas generally correlate with brown radiation stains that occur both in fractures and on the surface, although this is not always the case.

DISCUSSION

Effect of Irradiation on Marange Diamonds. Alpha particles (^{4}He ions) produced during ^{238}U, ^{235}U, and ^{232}Th decay result in radiation damage when they impact a diamond. These alpha particles have short penetration depths, so any damage is typically less than 30 µm into the diamond and results in green coloration (Crookes, 1904; Wagner, 1914; Lind and Barwell, 1923). Where this radiation damage and associated vacancy formation (V^0/GR1) are localized, green radiation stains (or spots) occur (Eaton-Magaña and Moe, 2016).

Diamonds with lower nitrogen content may be more likely to be damaged by radiation, as vacancy concentration has been shown to correlate with nitrogen content (Kiflawi et al., 2007). All 40 Marange

diamonds had high nitrogen contents, so any correlation between nitrogen content and vacancy concentration within this suite is unlikely.

Abundant radiation stains on the surfaces and within fractures indicate that the Marange diamonds were exposed to a radioactive source, likely during their >1 billion-year residency at the earth's surface. In natural diamonds, green radiation stains result when the diamond surface is in contact with minerals rich in uranium and thorium, such as uraninite (UO_2), for around 10 million years (Vance and Milledge, 1972). Zircons ($ZrSiO_4$) contain only trace amounts of uranium and would need to be in contact with diamond for significantly longer, around one billion years, to cause significant radiation damage to the diamond lattice (Nasdala et al., 2013).

Brown color in the radiation stains (figures 6 and 7) further indicates that these diamonds were heated to at least 600°C during their surface residency. Green radiation stains start changing to an olive color at 500–550°C and turn brown when heated to 600°C in the laboratory (Vance et al., 1973; Nasdala et al., 2013; Eaton-Magaña and Moe, 2016). Color change of the radiation stains from green to brown at 600°C is associated with loss of GR1, although the diamond lattice is expected to remain disordered and damaged (Nasdala et al., 2013).

Origin of Radiation and Metamorphism in the Marange Alluvial Deposit. Marange diamonds occur in Mesoproterozoic (>1.1 Ga) basal conglomerates of the Umkondo Group that comprise compositionally mature quartz pebble and cobble conglomerate (de Wit and Ward, 2014). The conglomerate also contains zircon and gold (de Wit and Ward, 2014). Given the long residency time of these diamonds at the surface, irradiation could have originated from either the Meso- to Paleoarchean basement gneisses of the Zimbabwe craton or from radioactive minerals (such as zircon) in the host Umkondo conglomerate. Although zircon contains significantly less uranium than uraninite, the billion-year residency of the diamonds in the conglomerate would be sufficient to cause green radiation stains (e.g., Nasdala et al., 2013). The Umkondo Group experienced greenschist to amphibolite facies metamorphism (Goodwin, 1996)—likely related to tectonic activity in the 0.55 Ga Mozambique Belt (see location in figure 1)—which would provide the requisite temperatures to change these green radiation spots to brown (Vance et al., 1973). Heating during metamorphism likely also facilitated the formation of the 594 nm and H3 (NVN^0) defects through vacancy migration, as well as formation of the NiN complexes (Lawson and Kanda, 1993).

Other Natural Diamonds with Abundant Radiation Stains. Apart from Marange, natural diamonds from many other localities show abundant radiation damage. Diamonds from the 2.8–2.9 Ga Central Rand Group of the Witwatersrand Basin (Kaapvaal craton, South Africa) show both green and brown radiation stains (Williams, 1932). Radiation damage to form the initially green radiation stains is consistent with these diamonds' occurrence in uraninite-rich conglomerate (Gittus, 1963; Raal and Robinson, 1980). Later heating events in the crust must have raised the temperatures to at least 600°C for these green stains to turn brown (Vance et al., 1973). These events could be related to either large-scale Bushveld magmatism at 2.1 Ga (see location on figure 1) or Karoo magmatism at the time of Gondwana breakup (~180 Ma).

Similarly, the majority of Guaniamo placer diamonds that occur in the alluvium of the Quebrada Grande River (Venezuela) have green radiation stains on their surface (Kaminsky et al., 2000; Schulze and Nasdala, 2016). The primary source for these diamonds are ~700 Ma kimberlite sills in the area (Kaminsky et al., 2000, 2004), and the lack of abundant brown radiation stains indicates there were no significant events that heated the crust more than 600°C. The source of radiation is still unknown, and radioactive grains could be related to Archean crust that is a potential source for monazite and zircon, or otherwise to the Guaniamo kimberlites that contain radioactive pyrochlore (Sharygin et al., 2009).

SUMMARY AND CONCLUSIONS

Although there are other occurrences of diamonds with natural radiation damage, the Marange locality may be unique in its high proportion of diamonds with abundant brown radiation stains that give them an almost black appearance. This could be due to their long residency (>1 Ga) in crustal conglomerates that contain highly radioactive minerals, followed by high-temperature metamorphism associated with the Mozambique belt (Goodwin, 1996).

Natural diamonds with Fancy black color grades and abundant radiation stains (such as the Marange samples studied here) are relatively easy to distinguish from any heat-treated or irradiated diamonds with similar color grades. Low-clarity diamonds that are highly fractured, such as the ones studied here, are not expected to survive HPHT treatment. However,

these fractured diamonds can be treated at LPHT conditions to graphitize the fractures and turn them into more valuable black diamonds (Hall and Moses, 2001; Notari, 2002). Such treatment would cause abundant graphitization along internal fractures, which is not visible in these Marange diamonds. Artificial irradiation is not expected to produce the radiation staining seen along the fractures, as this feature is most consistent with natural radioactive fluids infiltrating the fractures (figures 6 and 7).

Radiation stains and graphite needles are not the only cause of the dark appearance. A subset of the Marange diamonds contain abundant clouds of graphitic (+ methane) micro-inclusions in their cuboid sectors that impart a dark appearance to the bulk diamond, and these need to be distinguished from heated black diamonds that may have a similar appearance. Experiments by Eaton-Magaña et al. (2017) showed that the grain size of graphitic micro-inclusions in Marange diamonds increases during heat treatment, coinciding with the disappearance of any associated methane micro-inclusions. Accordingly, visual observations of graphite grain size, along with FTIR and Raman spectroscopy to detect methane, are required to distinguish natural from heat-treated Marange graphite-bearing diamonds.

ABOUT THE AUTHORS

Dr. Smit is a research scientist, and Ms. Myagkaya and Ms. Persaud are analytical technicians, at GIA in New York. Dr. Wang is GIA's vice president of research and development.

ACKNOWLEDGMENTS

We are grateful to Ulrika D'Haenens-Johansson for many useful discussions. Comments by Troy Ardon, Sally Eaton-Magaña, and Kyaw Soe Moe on an earlier version of this manuscript are appreciated. Eloïse Gaillou, Russell Shor, and Christopher Welbourn are thanked for constructive reviews that improved the final version of the manuscript. We are grateful to the DEYI Jewelry Company for making these samples available for study. Mike de Wit is thanked for informal discussions about the Marange diamond deposits.

REFERENCES

Ardon T. (2013) Lab Notes: Black diamond with unusual color origin. *G&G*, Vol. 49, No. 4, p. 252.

Benedetti L.R., Nguyen J.H., Caldwell W.A., Liu H., Kruger M., Jeanloz R. (1999) Dissociation of CH_4 at high pressures and temperatures: Diamond formation in giant planet interiors. *Science*, Vol. 286, pp. 100–102, http://dx.doi.org/10.1126/science.286.5437.100

Breeding C.M., Wang W. (2014) Characterization of gem diamonds from eastern Zimbabwe. Poster presentation at the 21st General Meeting of the International Mineralogical Association, Johannesburg.

Clark C.D., Ditchburn R.W., Dyer H.B. (1956) The absorption spectra of irradiated diamonds after heat treatment. *Proceedings of the Royal Society of London. Series A, Mathematical and Physical Sciences*, Vol. 237, No. 1208, pp. 75–89, http://dx.doi.org/10.1098/rspa.1956.0163

Clifford T.N. (1966) Tectono-metallogenic units and metallogenic provinces of Africa. *Earth and Planetary Science Letters*, Vol. 1, No. 6, pp. 421–434, http://dx.doi.org/10.1016/0012-821X(66)90039-2

Collins A.T. (1982) Colour centres in diamond. *Journal of Gemmology*, Vol. 18, No. 1, pp. 37–75, http://dx.doi.org/10.15506/JoG.1982.18.1.37

——— (1992) The characterisation of point defects in diamond by luminescence spectroscopy. *Diamond and Related Materials*, Vol. 1, No. 5-6, pp. 457–469, http://dx.doi.org/10.1016/0925-9635(92)90146-F

——— (2000) Spectroscopy of defects and transition metals in diamond. *Diamond and Related Materials*, Vol. 9, No. 3-6, pp. 417–423, http://dx.doi.org/10.1016/S0925-9635(99)00314-3

Collins A.T., Davies G., Woods G.S. (1986) Spectroscopic studies of the H1b and H1c absorption lines in irradiated, annealed type-Ia diamonds. *Journal of Physics C: Solid State Physics*, Vol. 19, No. 20, pp. 3933–3944, http://dx.doi.org/10.1088/0022-3719/19/20/026

Crookes W. (1904) On the action of radium emanation on diamonds. *Proceedings of the Royal Society of London*, Vol. 74, No. 497-506, pp. 47–49, http://dx.doi.org/10.1098/rspl.1904.0077

Dischler B. (2012) *Handbook of Spectral Lines in Diamond*. Springer, Berlin.

Dodson M.H., Compston W., Williams I.S., Wilson J.F. (1988) A search for ancient detrital zircons in Zimbabwean sediments. *Journal of the Geological Society, London*, Vol. 145, No. 6, pp. 977–983, http://dx.doi.org/10.1144/gsjgs.145.6.0977

Eaton-Magaña S.C., Moe K. (2016) Temperature effects on radiation stains in natural diamonds. *Diamond and Related Materials*, Vol. 64, pp. 130–142, http://dx.doi.org/10.1016/j.diamond.2016.02.009

Eaton-Magaña S., Ardon T., Zaitsev A.M. (2017) Inclusion and point defect characteristics of Marange graphite-bearing diamonds after high temperature annealing. *Diamond and Related Materials*, Vol. 71, pp. 20–29, http://dx.doi.org/10.1016/j.diamond.2016.11.011

Fisher D., Sibley S.J., Kelly C.J. (2009) Brown colour in natural di-

amond and interaction between the brown related and other colour-inducing defects. *Journal of Physics: Condensed Matter*, Vol. 21, No. 36, p. 364213, https://doi.org/10.1088/0953-8984/21/36/364213
Gittus J.H. (1963) *Metallurgy of the Rarer Metals-8. Uranium*. Butterworths, London.
Goodwin A. (1996) *Principles of Precambrian Geology*. Academic Press, London.
Goss J.P., Briddon P.R., Hill V., Jones R., Rayson M.J. (2014) Identification of the structure of the 3107 cm^{-1} H-related defect in diamond. *Journal of Physics: Condensed Matter*, Vol. 26, No. 14, 145801, http://dx.doi.org/10.1088/0953-8984/26/14/145801
Hainschwang T., Simic D., Fritsch E., Deljanin B., Woodring S., DelRe N. (2005) A gemological study of a collection of chameleon diamonds. *G&G*, Vol. 41, No. 1, pp. 20–35, http://dx.doi.org/10.5741/GEMS.41.1.20
Hall M., Moses T. (2001) Lab Notes: Heat-treated black diamond: Before and after. *G&G*, Vol. 37, No. 3, pp. 214–215.
Hanson R.E., Crowley J.L., Bowring S.A., Ramezani J., Gose W.A., Dalziel I.W.D., Pancake J.A., Siedel E.K., Blenkinsop T.G., Mukwakwami J. (2004) Coeval large-scale magmatism in the Kalahari and Laurentian cratons during Rodinia assembly. *Science*, Vol. 304, No. 5674, pp. 1126–1129, http://dx.doi.org/10.1126/science.1096329
Hanson R.E., Rioux M., Gose W.A., Blackburn T.J., Bowring S.A., Mukwakwami J., Jones D.L. (2011) Paleomagnetic and geochronological evidence for large-scale post-1.88 Ga displacement between the Zimbabwe and Kaapvaal cratons along the Limpopo belt. *Geology*, Vol. 39, No. 5, pp. 487–490, http://dx.doi.org/10.1130/G31698.1
Howell D., Griffin W.L., Piazolo S., Say J.M., Stern R.A., Stachel T., Nasdala L., Rabeau J.R., Pearson N.J., O'Reilly S.Y. (2013) A spectroscopic and carbon-isotope study of mixed-habit diamonds: Impurity characteristics and growth environment. *American Mineralogist*, Vol. 98, No. 1, pp. 66–77, http://dx.doi.org/10.2138/am.2013.4179
Iakoubvskii K., Adriaenssens G.J. (2002) Optical characterization of natural Argyle diamonds. *Diamond and Related Materials*, Vol. 11, No. 1, pp. 125–131, http://dx.doi.org/10.1016/S0925-9635(01)00533-7
Jacobs J., Pisarevsky S., Thomas R.J., Becker T. (2008) The Kalahari Craton during the assembly and dispersal of Rodinia. *Precambrian Research*, Vol. 160, No. 1-2, pp. 142–158, http://dx.doi.org/10.1016/j.precamres.2007.04.022
Johnston K., Mainwood A. (2003) Properties of nickel nitrogen complexes in diamond: stability and electronic structure. *Diamond and Related Materials*, Vol. 12, No. 3-7, pp. 516–520, http://dx.doi.org/10.1016/S0925-9635(02)00389-8
Kaminsky F.V., Zakharchenko O.D., Griffin W.L., Channer D.M.D.R., Khachatryan-Blinova G.K. (2000) Diamond from the Guaniamo area, Venezuela. *Canadian Mineralogist*, Vol. 38, No. 6, pp. 1347–1370, http://dx.doi.org/10.2113/gscanmin.38.6.1347
Kaminsky F.V., Sablukov S.M., Sablukova L.I., Channer D.M.D.R. (2004) Neoproterozoic 'anomalous' kimberlites of Guaniamo, Venezuela: mica kimberlites of 'isotopic transitional' type. *Lithos*, Vol. 76, No. 1-4, pp. 565–590, http://dx.doi.org/10.1016/j.lithos.2004.03.035
Kiflawi I., Collins A.T., Iakoubvskii K., Fisher D. (2007) Electron irradiation and the formation of vacancy-interstitial pairs in diamond. *Journal of Physics: Condensed Matter*, Vol. 19, No. 4, 046216, http://dx.doi.org/10.1088/0953-8984/19/4/046216
Kitawaki H. (2007) Gem diamonds: Causes and colors. *New Diamond and Frontier Carbon Technology*, Vol. 17, pp. 119–126.
Lang A.R., Yelisseyev A.P., Pokhilenko N.P., Steeds J.W., Wotherspoon A. (2004) Is dispersed nickel in natural diamonds associated with cuboid growth sectors in diamonds that exhibit a history of mixed-habit growth? *Journal of Crystal Growth*, Vol. 263, No. 1-4, pp. 575–589, http://dx.doi.org/10.1016/j.jcrysgro.2003.11.116
Lawson S.C., Kanda H. (1993) An annealing study of nickel point defects in high-pressure synthetic diamond. *Journal of Applied Physics*, Vol. 73, No. 8, pp. 3967–3973, http://dx.doi.org/10.1063/1.352861
Lind S.C., Barwell D.C. (1923) The coloring and thermophosphorescence produced in transparent minerals and gems by radium radiation. *American Mineralogist*, Vol. 8, pp. 171–180.
McCourt S., Kampunzu A.B., Bagai Z., Armstrong R.A. (2004) The crustal architecture of Archaean terranes in northeastern Botswana. *South African Journal of Geology*, Vol. 107, No. 1-2, pp. 147–158, http://dx.doi.org/10.2113/107.1-2.147
Moore A.E., Cotterill F.P.D., Broderick T., Plowes D. (2009) Landscape evolution in Zimbabwe from the Permian to present, with implications for kimberlite prospecting. South African *Journal of Geology*, Vol. 112, No. 1, pp. 65–88, http://dx.doi.org/10.2113/gssajg.112.1.65
Nadolinny V.A., Yelisseyev A.P., Baker J.M., Newton M.E., Twitchen D.J., Lawson, S.C., Yuryeva O.P., Feigelson B.N. (1999) A study of ^{13}C hyperfine structure in the EPR of nickel-nitrogen-containing centres in diamond and correlation with their optical properties. *Journal of Physics: Condensed Matter*, Vol. 11, No. 38, pp. 7357–7376, http://dx.doi.org/10.1088/0953-8984/11/38/314
Nägler T.F., Kramers J.D., Kamber B.S., Frei R., Prendergast M.D.A. (1997) Growth of subcontinental lithospheric mantle beneath Zimbabwe started at or before 3.8 Ga: Re-Os study on chromites. *Geology*, Vol. 25, No. 11, pp. 983–986, http://dx.doi.org/10.1130/0091-7613(1997)025%3C0983:GOSLMB%3E2.3.CO;2
Nasdala L., Grambole D., Wildner M., Gigler A.M., Hainschwang T., Zaitsev A.M., Harris J.W., Milledge J., Schulze D.J., Hofmeister W., Balmer W.A. (2013) Radio-colouration of diamond: a spectroscopic study. *Contributions to Mineralogy and Petrology*, Vol. 165, No. 5, pp. 843–861, http://dx.doi.org/10.1007/s00410-012-0838-1
Nazaré M.H., Neves A.J., Davies G. (1991) Optical studies of the 1.40 eV Ni center in diamond. *Physical Review B*, Vol. 43, No. 17, pp. 14196–14205, http://dx.doi.org/10.1103/PhysRevB.43.14196
Newton M. (2011) Treated diamond identification. *G&G*, Vol. 47, No. 2, p. 106.
Notari F. (2002) Traitement du diamant noir por graphitation "interne" [Treatment of black diamond by internal graphitization]. *Revue de Gemmologie a.f.g.*, No. 145-146, pp. 42–60.
Raal F.A., Robinson D.N. (1980) Green for rarity. *Nuclear Active*, Vol. 23, pp. 5–8.
Rakovan J., Gaillou E., Post J E., Jaszczak J.A., Betts J.H. (2014) Optically sector-zoned (star) diamonds from Zimbabwe. *Rocks and Minerals*, Vol. 89, No. 2, pp. 173–178, http://dx.doi.org/10.1080/00357529.2014.842844
Rondeau B., Fritsch E., Guiraud M., Chalain J.-P., Notari F. (2004) Three historical 'asteriated' hydrogen-rich diamonds: growth history and sector-dependent impurity incorporation. *Diamond and Related Materials*, Vol. 13, No. 9, pp. 1658–1673, http://dx.doi.org/10.1016/j.diamond.2004.02.002
Rubanova E.V., Palazhchenko O.V., Garanin V.K. (2009) Diamonds from the V. Grib pipe, Arkhangelsk kimberlite province, Russia. *Lithos*, Vol. 112S, pp. 880–885, http://dx.doi.org/10.1016/j.lithos.2009.04.044
Schulze D.J., Nasdala L. (2016) Unusual paired pattern of radiohaloes on a diamond crystal from Guaniamo (Venezuela). *Lithos*, Vol. 265, http://dx.doi.org/10.1016/j.lithos.2016.09.024
Sharygin V.V., Sobolev N.V., Channer D.M.D.R. (2009) Oscillatory-zoned crystals of pyrochlore-group minerals from the Guaniamo kimberlites. *Lithos*, Vol. 112S, pp. 976–985, http://dx.doi.org/10.1016/j.lithos.2009.03.049
Smit K.V., Shirey S.B., Stern R.A., Steele A., Wang W. (2016) Diamond growth from C–H–N–O recycled fluids in the lithosphere: Evidence from CH_4 micro-inclusions and $\delta^{13}C$–$\delta^{15}N$–N content in Zimbabwe mixed-habit diamonds. *Lithos*, Vol. 265,

pp. 68–81, http://doi.org/10.1016/j.lithos.2016.03.015
Stowe C.W. (1989) The Proterozoic Magondi mobile belt in Zimbabwe; discussion. *South African Journal of Geology*, Vol. 92, No. 1, pp. 69–71.
Teinturier S., Pironon J., Walgenwitz F. (2002) Fluid inclusions and PVTX modelling: examples from the Garn Formation in well 6507/2-2, Haltenbanken, Mid-Norway. *Marine and Petroleum Geology*, Vol. 19, No. 6, pp. 755–765, http://dx.doi.org/10.1016/S0264-8172(02)00055-7
Titkov S.V., Zudin N.G., Gorshkov A.I., Sivtsov A.V., Magazina L.O. (2003) An investigation into the cause of color in natural black diamonds from Siberia. *G&G*, Vol. 39, No. 3, pp. 200–209, http://dx.doi.org/10.5741/GEMS.39.3.200
Vance E.R., Milledge H.J. (1972) Natural and laboratory α-particle irradiation of diamond. *Mineralogical Magazine*, Vol. 38, No. 299, pp. 878–881, http://dx.doi.org/10.1180/minmag.1972.038.299.11
Vance E.R., Harris J.W., Milledge H.J. (1973) Possible origins of α-damage in diamonds from kimberlite and alluvial sources. *Mineralogical Magazine*, Vol. 39, No. 303, pp. 349–360, http://dx.doi.org/10.1180/minmag.1973.039.303.12
Wagner P.A. (1914) *The Diamond Fields of Southern Africa*. Transvaal Leader, Johannesburg.
Welbourn C.M., Rooney M.T., Evans D.J.F. (1989) A study of diamonds of cube and cube-related shape from the Jwaneng mine. *Journal of Crystal Growth*, Vol. 94, pp. 229–252, http://dx.doi.org/10.1016/0022-0248(89)90622-2
Welbourn C.M., Cooper M., Spear P.M. (1996) De Beers natural versus synthetic diamond verification instruments. *G&G*, Vol. 32, No. 3, pp. 156–169, http://dx.doi.org/10.5741/GEMS.32.3.156
Williams A.F. (1932) *The Genesis of the Diamond II*. Ernest Benn Ltd., London.
Wilson J.F. (1990) A craton and its cracks: some of the behaviour of the Zimbabwe block from the Late Archaean to the Mesozoic in response to horizontal movements, and the significance of some of its mafic dyke fracture patterns. *Journal of African Earth Sciences*, Vol. 10, No. 3, pp. 483–501, http://dx.doi.org/10.1016/0899-5362(90)90101-J
de Wit M., Ward J. (2014) The Proterozoic Marange alluvial diamond deposit in eastern Zimbabwe: Is this a Mega-placer? Vancouver Kimberlite Cluster seminar, University of British Columbia, March 7.
van Wyk J.A. (1982) Carbon-12 hyperfine interaction of the unique carbon of the P2 (ESR) or N3 (optical) centre in diamond. *Journal of Physics C: Solid State Physics*, Vol. 15, No. 27, pp. L981–L983, http://dx.doi.org/10.1088/0022-3719/15/27/007
Yelisseyev A., Kanda H. (2007) Optical centers related to 3d transition metals in diamond. *New Diamond and Frontier Carbon Technology*, Vol. 17, No. 3, 127–178.
Zeh A., Gerdes A., Barton J.M. (2009) Archean accretion and crustal evolution of the Kalahari craton—the zircon age and Hf isotope record of granitic rocks from Barberton/Swaziland to the Francistown Arc. *Journal of Petrology*, Vol. 50, No. 5, pp. 933–966, http://dx.doi.org/10.1093/petrology/egp027
Zeh A., Jaguin J., Poujol M., Boulvais P., Block S., Paquette J.-L. (2013) Juvenile crust formation in the northeastern Kaapvaal Craton at 2.97 Ga—Implications for Archean terrane accretion, and the source of the Pietersburg gold. *Precambrian Research*, Vol. 233, pp. 20–43, http://dx.doi.org/10.1016/j.precamres.2013.04.013
Zeh A., Stern R.A., Gerdes A. (2014) The oldest zircons of Africa—Their U–Pb–Hf–O isotope and trace element systematics, and implications for Hadean to Archean crust–mantle evolution. *Precambrian Research*, Vol. 241, pp. 203–230, http://dx.doi.org/10.1016/j.precamres.2013.11.006